ChemComm

COMMUNICATION

View Article Online
View Journal | View Issue

Cite this: *Chem. Commun.*, 2024, **60**, 3198

Received 6th January 2024,
Accepted 21st February 2024

DOI: 10.1039/d4cc00083h

rsc.li/chemcomm

An electrospun three-layer nanofibrous membrane-based *in situ* gel separator for efficient lithium-organic batteries†

Mingyu Yin,[a] Xi Liu,[ac] *Caiting Li,[a] Deyi Liao,[a] Yichao Yang,[a] Shaobo Han,*[a] Longfei Fan,[a] Jing Zhao,[a] Hui Yu,[a] Qingguang Zeng[bc] and Da Wang[bc] *

An *in situ* gel separator based on an electrospun three-layer nanofibrous membrane (PSE11-Gel) is developed for high-performance lithium-organic batteries (LOBs). The highly efficient shuttle effect inhibition of organic cathode molecules or lithiated intermediates has been demonstrated for PSE11-Gel to realize high-capacity stable LOBs.

In recent years, organic cathode materials (OCMs) for lithium organic batteries (LOBs) have attracted more and more attention due to their diverse chemical structures, low production cost, and green and renewable characteristics.[1–3] Meanwhile, to achieve high theoretical specific capacities, OCMs usually require low molecular weights, which brings certain challenges to the corresponding LOBs.[4] One of the most striking features of small-molecule OCMs is that their intrinsic molecules, or redox intermediates, are readily soluble in conventional electrolytes.[5–7] The organic small molecules dissolved in the electrolyte tend to pass through the separator, resulting in a shuttle effect that can deteriorate or even damage the battery.[5–7] Many strategies have been adopted to tackle the dissolution issues and shuttle effects of OCMs, including polymerization engineering of cathode materials and optimization of separator and electrolyte species.[4,8] For example, Yoshida *et al.* reported that the polymethacrylate-derived polymer linked pyrene-4,5,9,10-tetraone (PYT) side chain-based cathode exhibited a similar capacity and remarkably improved cycling stability compared to the cathode of the PYT molecule.[9] Our group demonstrated that a low-cost carbonyl polymer cathode, poly(piperazine-benzoquinone), can be obtained from the polymerization of vanillin and piperazine under oxidative amination, exhibiting a high reversible capacity of 257 mA h g^{-1}, as well as much higher cycling stability than its small molecule-based cathode.[7]

Chemically speaking, polymerized organic cathode molecules inevitably introduce non-electrochemical active components into the molecular formulas, which is not conducive for maximizing the theoretical specific capacities of OCMs. Therefore, optimizing the separators acts as one feasible solution to solve this problem of high theoretical specific capacity of OCMs.[10,11] For example, Song *et al.* reported a series of polypropylene/Nafion/polypropylene (PNP) sandwich-type separators, and the related LOB showed dramatically improved cycling stability when the PNP5 separator was applied.[12] Pan *et al.* prepared ion selective separators based on graphene oxide, showing the abilities of lithium ion transport and electroactive organic anion rejection, which stabilized lithium organic batteries.[13] Jonson *et al.* demonstrated that lithium garnet separators can block the soluble small-molecule quinone's crossover, suggesting a promising approach to enable high capacities with soluble OCMs.[14] Wu *et al.* proposed a multifunctional Janus separator for organic cathode-based batteries to achieve high capacity and remarkable cycling performance applications.[15] In addition to preparing multilayer or hybrid modified separators, researchers have further paid attention to developing gel composite separators by drawing on the design strategies of quasi-solid-state batteries.[16,17] For example, Bai *et al.* reported on the use of a metal–organic framework composite gel membrane as a separator to develop LOBs with high energy density and long cycling life.[16] Li *et al.* demonstrated that a gel polymer electrolyte can be *in situ* obtained on Nafion-coated separators to eliminate the shuttle effect for LOBs, offering the electrochemical performance of long cycle life and high rate.[17] Indeed, these reported multilayer or gel separators have shown good performance characteristics in LOBs. However, the Nafion used in their preparation is expensive, hindering their future large-scale applications.[18] Therefore, it is of great significance to develop composite separators with a simple preparation process, low-cost production, and excellent electrochemical performance.

In this work, we report an *in situ* gel separator (PSE11-Gel) based on a three-layer nanofibrous membrane (PSE11), which effectively

[a] *College of Textile Science and Engineering, Wuyi University, Jiangmen 529020, China. E-mail: liuxi@wyu.edu.cn, hanshaobo@wyu.edu.cn*
[b] *School of Applied Physics and Materials, Wuyi University, Jiangmen, 529020, China. E-mail: dawang@mail.ustc.edu.cn*
[c] *Institute of Carbon Peaking and Carbon Neutralization, Wuyi University, Jiangmen, 529020, China*

† Electronic supplementary information (ESI) available. See DOI: https://doi.org/10.1039/d4cc00083h

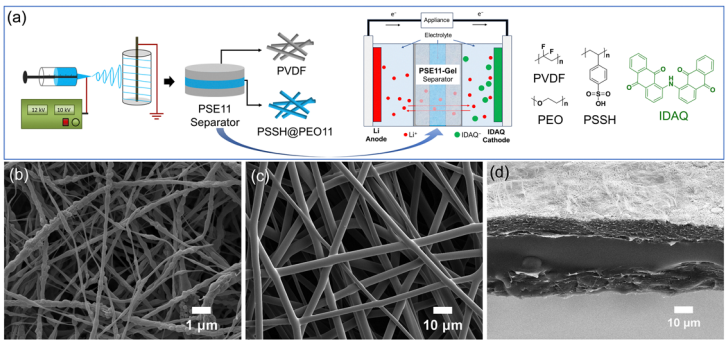

Fig. 1 (a) Schematic diagram of the preparation of PSE11, and its application in LOBs; as well as the related chemical structures of the polymers and OCM. SEM images of PVDF (b) and PSSH@PEO11 (c) nanofibers, and the sectional view of the PSE11 separator (d).

inhibited the shuttle effect of OCM. A schematic of the preparation is shown in Fig. 1a. First, PSE11 was prepared by sequential electrospinning of poly(vinylidene fluoride) (PVDF), poly(styrene sulfonic acid)@poly(ethylene oxide) (1 : 1 wt./wt.) (PSSH@PEO11), and PVDF. Then PSE11-Gel was formed *in situ* in a battery with PSE11 as the separator, which is attributed to the 1,3-dioxolane (DOL) molecules in the electrolyte being attacked by the side chain of PSSH in PSE11 to produce the poly(1,3-dioxolane) (PDOL) gel by ring-opening polymerization. Moreover, the polymers (PVDF, PSSH, and PEO) used in this preparation are more cost-effective than reported Nafion-based systems. Importantly, PSE11-Gel exhibits the characteristics of efficient Li^+ transport and an organic small molecular barrier. Compared to the conventional (Celgard 2400) and non-gel nanofiber (PVDF) separator-based LOBs, using a conventional OCM (IDAQ)-based cathode, the PSE11-Gel-based LOB exhibits the highest cycling stability (keep 180–240 mA h g^{-1} capacity over 200 cycles) and excellent rate performance ($\approx$ 180 mA h g^{-1} capacity at 500 mA g^{-1}). This study provides a simple and efficient strategy for realizing gel nanofiber composite separators for high-performance and stable LOBs.

The Fourier-transform infrared (FTIR) curve of the PSSH@PEO nanofiber membrane (Fig. S1, ESI†) shows the overlay of the characteristic peaks of pure PSSH and PEO polymers, verifying that the chemical structures of the two polymers were well maintained during electrospinning. In particular, the PSSH@PEO11 nanofiber membrane exhibits the presence of sulfonic acid of PSSH at 1030 and 1002 cm^{-1}, ensuring its ability to act as a proton catalyst to catalyze the polymerization of DOL into a gel composite membrane.[19] Meanwhile, the PEO phase in PSSH@PEO11 shows a structure similar to that of the polymer with the ring-opening polymerization of DOL, indicating that the structure of the PEO11 backbone was maintained after polymerization.

The morphologies of the corresponding electrospun nanofibers were studied by scanning electron microscopy (SEM). As shown in Fig. 1b–d, three-layer nanofibrous membrane PSE11 prepared by electrospinning presents a good three-dimensional network microfiber structure. Specifically, the upper and lower nanofibers electrospun by pure PVDF show a uniform three-dimensional (3D) network nanofibrous morphology with an average nanofiber diameter of $\approx$140 nm (Fig. S2a, ESI†). Moreover, due to the intrinsic moderate molecular rigidity of PVDF, the single nanofiber of PVDF nanofibrous membrane displays a certain rough and quasi-beaded surface morphology.[20] The fine nanostructures of the PVDF nanofibers will contribute to their functions as the outer layers of the three-layer nanofibrous membrane for efficient lithium-ion conduction. The middle layer of PSE11, PSSH@PEO11, presents a uniform 3D smooth fiber morphology with an average diameter of $\approx$3.8 μm (Fig. S2b, ESI†). The thicker fibers presented by PSSH@PEO11, compared to the PVDF nanofibers, may be caused by the use of two polymers with softer main chains during its electrospinning preparation. Fig. 1d shows the result of the sectional SEM measurement on the PSE11 separator, where the sandwich structure of the three-layer composite nanofibrous membrane can be observed. The thickness of the PVDF nanofiber layer, PSSH@PEO11 layer, and PVDF nanofiber layer is about 10, 20, and 10 μm, respectively, demonstrating that a 40 μm-thick sandwich-like nanofibrous separator has been successfully prepared by electrospinning and rolled treatment. Meanwhile, the control PVDF and Celgard 2400 separators are 32 and 23 μm, respectively (Fig. S3, ESI†), suggesting that the thickness of the electrospun prepared three-layer PSE11 separator is appropriate. It should be noted that, before rolled treatment of the fresh PSE11, the PVDF nanofibers display fleecy structures on both sides and the structure of the PSSH@PEO11 is relatively compact (Fig. S4, ESI†), which may be due to the different softness of the PVDF and PSSH/PEO polymers. Overall, the PSSH@PEO11 layer can bond the fluffy PVDF nanofiber membranes on both sides firmly, ensuring good mechanical properties of the electrospun PSE11 separator (Fig. S5, ESI†).

Considering the micron-level pore size presented in the morphology of the electrospun PSE11 membrane, it is difficult to achieve an effective barrier at the organic molecular level as a separator. To further validate our design strategy of DOL ring-opening polymerization to form a composite gel based on PSE11 containing PSSH@PEO11 nanofibers, we performed electrolyte immersion experiments with the relevant nanofiber membranes. As shown in Fig. 2a, the 1.0 M LiTFSI (DOL/DME 1 : 1 v/v) electrolyte (0.5 mL) soaked with PSE11 membrane gradually formed a white opaque gel over 24 hours and finally appeared to be in a pale white quasi-solid state (Fig. S6, ESI†). However, after 24 hours, the electrolyte soaked with pure PVDF nanofiber membrane remained in solution (Fig. 2b). SEM tests on the surface (Fig. 2c and d) and cross-section (Fig. 2e) of the PSE11-based quasi-solid gel were also carried out, and the formation of the whole gel (PSE11-Gel) was confirmed from

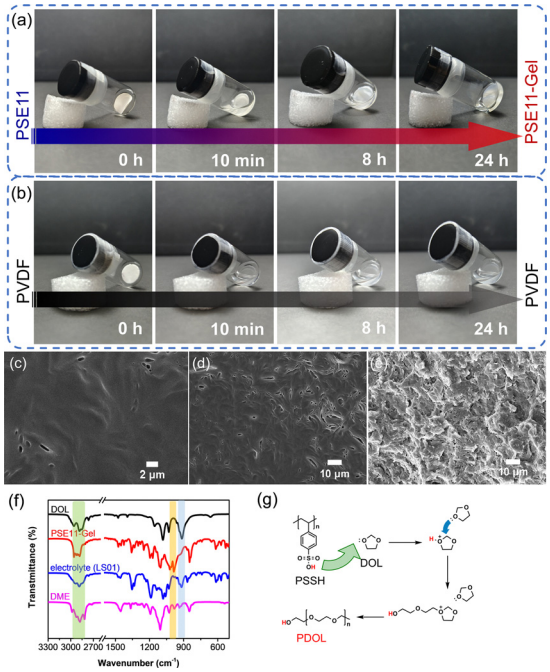

Fig. 2 Optical photographs of the liquid electrolyte soaked with PSE11 (a) and PVDF (b) membranes. SEM images of the surface (c) and (d) and cross-section (e) of the PSE11-gel. (f) FTIR spectra of the PSE11-Gel, electrolyte, and the corresponding solvents. (g) The corresponding proposed reaction process of the ring-opening polymerization of DOL (PDOL).

the morphology. Furthermore, to investigate the composition of this composite gel, we performed FTIR measurements of the corresponding PSE11-gel, electrolyte, and solvents (DME and DOL). Compared with the electrolyte and solvent, the infrared characteristic peaks of PSE11-Gel (Fig. 2f) at ≈3000, 912, and 840 cm^{-1} indicate the disappearance of the –O–CH_2–O-bond in small molecules, preliminarily confirming our design strategy for DOL ring-opening polymerization to form the nanofibrous gel.[17,21–23] Gel permeation chromatography (GPC) and mass (MALDI-TOF) spectrum measurements (Fig. S7 and S8, ESI†) showed that the PSE11-Gel has a number-average molecular weight (Mn) of ~60 kDa and a polydispersity index (PDI) of ~1.3. Therefore, combined with the relevant ^{1}H-NMR results (Fig. S9, ESI†), we speculate that the PSE11-gel was formed by catalyzed ring-opening polymerization induced from PSSH side-chain proton H, and the corresponding proposed reaction process is shown in Fig. 2g.[17]

The ability of PSE11-Gel to be used as a separator was evaluated through cyclic voltammetry (CV) and battery measurements. 2032-Type half-cells were assembled using the commercial IDAQ-based cathode, 1.0 M LiTFSI (DOL/DME 1 : 1 v/v) electrolyte, and lithium foil anode. PSE11 nanofibrous membrane acts as a separator, of which the *in situ* gel separator (PSE11-Gel) formed during the settling process of the battery. Conventional commercial membrane (Celgard 2400) and PVDF nanofibrous membrane separator-based batteries were also assembled for comparison. The similar CV curves of the IDAQ-based cathodes in the voltage range of 1.5–3.0 V with the three separators, preliminarily suggest the basic separator property of PSE11-Gel for battery fabrication (Fig. 3a). The good reversible oxidation and reduction peaks at 1.7–2.5 V verified the electrochemical behavior of IDAQ, which indicated that the electrochemical properties of the organic cathode were not affected during the *in situ* gel formation of PSE11-Gel.

The results of discharge/charge tests are shown in Fig. 3b. The corresponding LOBs exhibit an initial specific capacity of 239, 236, and 244 mA h g^{-1} with PSE11-Gel, PVDF, and Celgard 2400 as the separators, respectively, which are all close to the theoretical capacity of IDAQ (250 mA h g^{-1}). Although the initial specific capacities of the three separator-based batteries are relatively similar, their cycling performance (Fig. 3c) shows significant differences. After 200 cycles, the PSE11-Gel-based battery shows a 70% capacity retention, while only 28% and 26% capacity retention for PVDF and Celgard 2400-based batteries. Meanwhile, the PSE11-Gel-based battery showed almost 100% Coulombic efficiency, while the PVDF and Celgard 2400-based batteries' Coulombic efficiencies were among 80–90%, indicating the highest reversibility and stability for the PSE11-Gel-based battery. This result suggested that PSE11-Gel inhibits the shuttle effect of pristine and/or lithiated IDAQ during the discharge/charge process of LOBs.

The rate properties of these three separator-based batteries were further measured at various current densities (Fig. 3d). The PSE11-Gel-based battery showed reversible capacities of 240, 220, 204, and 180 mA h g^{-1} at 100, 200, 300, and 500 mA g^{-1}, respectively. When the current rate returned to 100 mA g^{-1}, the capacity recovered to 196 mA h g^{-1}. By contrast, the PVDF- and Celgard 2400-based batteries showed relatively low rate performance, showing capacities of 55–80% of the PSE11-Gel-based battery performance at different current densities. Meanwhile, the applicability of the PSE11-Gel separator was preliminarily verified by evaluating the highly active material load and various cathode batteries (Fig. S10, ESI†).[17,24] Overall, the electrochemical performance indicated that the PSE11-Gel separator is a good solution for fabricating high-performance and stable LOBs.

To further visualize the effect of the PSE11-Gel separator on inhibiting the shuttle effect of organic molecules or lithiated

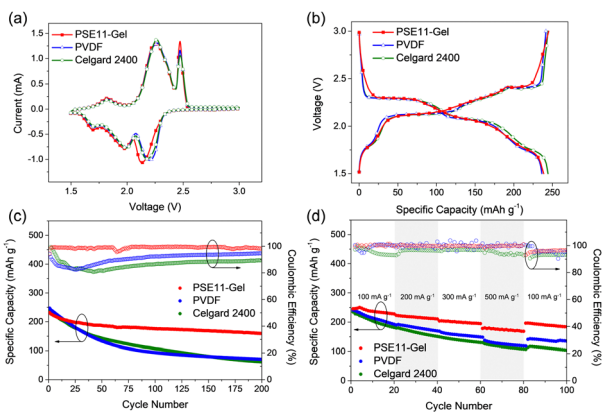

Fig. 3 (a) CV curves of IDAQ-based cathodes with three separators at 0.1 mV s^{-1}. Galvanostatic discharge/charge curves (b), cycling stabilities (c) and rate performance (d) of IDAQ-based batteries with three separators.

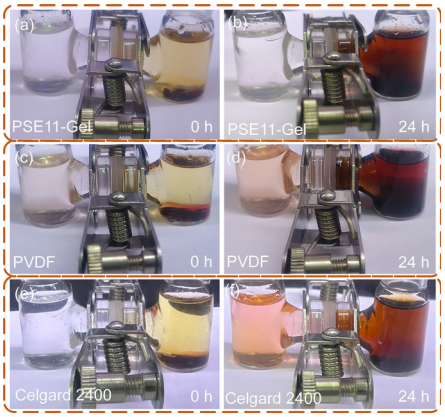

Fig. 4 Photographs of the visual penetration tests of the lithiated IDAQ with PSE11-Gel (a) and (b), PVDF (c) and (d), and Celgard 2400 (e) and (f) as the separator.

intermediates, the relevant H-shaped tube penetration experiments were studied. The electrolytes soaked with *ex situ* IDAQ cathodes (discharged to 2.1 V) were loaded to one side of the H-shaped tubes, and an equal amount of electrolytes were loaded to the other sides (Fig. 4). PSE11-Gel, PVDF, and Celgard 2400 separators were respectively inserted in the middle of the H-shaped tubes. After 24 h, more obvious brown solutions were seen on the pure electrolyte-loaded sides of the PVDF and 2400-based separated H-shaped tubes. Excitingly, the solution of colored organic molecules or lithiated intermediates can barely penetrate the PSE11-Gel separator, confirming its highly efficient inhibition of the shuttle effect of OCMs for excellent battery performance. Combined with the above study on the formation mechanism of PSE11-Gel based on DOL ring-opening polymerization, the efficient shuttle-blocking effect of PSE11-Gel can be attributed to the gelatinized membrane structure and the rejection of the lithiated intermediates by a large number of sulfonic anions remaining in the gel.[25,26]

In conclusion, we demonstrated an *in situ* formed gel separator based on electrospun three-layer nanofibers for inhibiting the shuttle effect of OCMs to realize high-performance and stable LOBs. The sandwich-like three-layer nanofibrous PSE11 membrane was prepared by sequential electrospinning of PVDF, PSSH@PEO, and PVDF. A gel nanofiber composite separator, PSE11-Gel, was formed *in situ* in a battery with PSE11 as the separator. Specifically, the DOL molecules in the electrolyte were attacked by the side chain of PSSH in PSE11 to produce the PDOL gel by ring-opening polymerization, showing a gel-like composite separator. PSE11-Gel not only exhibits the characteristics of efficient Li^+ transport but also serves as an organic small molecular barrier. Compared to Celgard 2400 and non-gel PVDF nanofiber separator-based LOBs, the PSE11-Gel-based LOB exhibits superior cycling stability and excellent rate performance. Meanwhile, the measurement of the high active material load and various cathode batteries preliminarily verified the applicability of the PSE11-Gel separator. This study provides a simple and efficient strategy for realizing gel nanofiber composite separators for high-performance LOBs.

Mingyu Yin: investigation, data curation. Xi Liu: supervision, conceptualization, writing – review & editing, project administration. Caiting Li: investigation, data curation. Deyi Liao: investigation. Yichao Yang: investigation. Shaobo Han: formal analysis, writing – review & editing. Longfei Fan: writing – review & editing. Jing Zhao: writing – review & editing. Hui Yu: resources. Qingguang Zeng: resources. Da Wang: methodology, validation, writing – review & editing.

This work was supported by the National Natural Science Foundation of China (No. 22005224, 21975187, and 52003202), and Guangdong Key Building Discipline Research Capability Enhancement Funds (2021ZDJS093). The research was also financially supported by the Science Foundation for High-level Talents of Wuyi University (AL2019003 and 2018TP031) and Wuyi University–Hong Kong/Macau Joint Research Funds (2019WGALH02).

Conflicts of interest

There are no conflicts to declare.

Notes and references

1 P. Poizot, J. Gaubicher, S. Renault, L. Dubois, Y. Liang and Y. Yao, *Chem. Rev.*, 2020, **120**, 6490–6557.
2 Y. Lu and J. Chen, *Nat. Rev. Chem.*, 2020, **4**, 127–142.
3 T. P. Nguyen, A. D. Easley, N. Kang, S. Khan, S.-M. Lim, Y. H. Rezenom, S. Wang, D. K. Tran, J. Fan, R. A. Letteri, X. He, L. Su, C.-H. Yu, J. L. Lutkenhaus and K. L. Wooley, *Nature*, 2021, **593**, 61–66.
4 Y. Lu, Q. Zhang, L. Li, Z. Niu and J. Chen, *Chemistry*, 2018, **4**, 2786–2813.
5 Z. Song, Y. Qian, T. Zhang, M. Otani and H. Zhou, *Adv. Sci.*, 2015, **2**, 1500124.
6 V. W.-h Lau, I. Moudrakovski, J. Yang, J. Zhang and Y.-M. Kang, *Angew. Chem., Int. Ed.*, 2020, **59**, 4023–4034.
7 C. Li, X. Liu, Z. He, W. Tao, Y. Zhang, Y. Zhang, Y. Jia, H. Yu, Q. Zeng, D. Wang, J. H. Xin, C. Duan and F. Huang, *J. Power Sources*, 2021, **511**, 230464.
8 D. Xu, M. Liang, S. Qi, W. Sun, L.-P. Lv, F.-H. Du, B. Wang, S. Chen, Y. Wang and Y. Yu, *ACS Nano*, 2021, **15**, 47–80.
9 T. Nokami, T. Matsuo, Y. Inatomi, N. Hojo, T. Tsukagoshi, H. Yoshizawa, A. Shimizu, H. Kuramoto, K. Komae, H. Tsuyama and J.-I. Yoshida, *J. Am. Chem. Soc.*, 2012, **134**, 19694–19700.
10 Y. Pan, S. Chou, H. K. Liu and S. X. Dou, *Natl. Sci. Rev.*, 2017, **4**, 917–933.
11 F. Qi, Z. Sun, X. Fan, Z. Wang, Y. Shi, G. Hu and F. Li, *Adv. Energy Mater.*, 2021, **11**, 2100387.
12 Z. Song, Y. Qian, M. Otani and H. Zhou, *Adv. Energy Mater.*, 2016, **6**, 1501780.
13 Y. Pan, J. Hao, X. Zhu, Y. Zhou and S.-L. Chou, *Inorg. Chem. Front.*, 2018, **5**, 1869–1875.
14 R. A. Jonson, V. S. Battaglia and M. C. Tucker, *ACS Appl. Energy Mater.*, 2023, **6**, 745–752.
15 Y. Wu, X. Wang, F. Zhang, L. Hai, Q. Chen, C. Chao, A. Yang, Y. Sun and D. Jia, *Adv. Funct. Mater.*, 2023, 2309552.
16 S. Bai, B. Kim, C. Kim, O. Tamwattana, H. Park, J. Kim, D. Lee and K. Kang, *Nat. Nanotechnol.*, 2021, **16**, 77–84.
17 M. Li, J. Yang, Y. Shi, Z. Chen, P. Bai, H. Su, P. Xiong, M. Cheng, J. Zhao and Y. Xu, *Adv. Mater.*, 2022, **34**, 2107226.
18 K. A. Mauritz and R. B. Moore, *Chem. Rev.*, 2004, **104**, 4535–4586.
19 P. Li, N. Su, Z. Wang and J. Qiu, *ACS Nano*, 2021, **15**, 16811–16818.
20 Y. Wu, Y. Li, Y. Wang, Q. Liu, Q. Chen and M. Chen, *J. Energy Chem.*, 2022, **64**, 62–84.
21 Q. Zhao, X. Liu, S. Stalin, K. Khan and L. A. Archer, *Nat. Energy*, 2019, **4**, 365–373.
22 S. Yang, Z. Liu, Y. Liu and Y. Jiao, *J. Mater. Sci.*, 2015, **50**, 1544–1552.
23 M. Li, R. P. Hicks, Z. Chen, C. Luo, J. Guo, C. Wang and Y. Xu, *Chem. Rev.*, 2023, **123**, 1712–1773.
24 Z. Gong, S. Zheng, J. Zhang, Y. Duan, Z. Luo, F. Cai and Z. Yuan, *ACS Appl. Mater. Interfaces*, 2022, **14**, 11474–11482.
25 D. B. Babu, K. Giribabu and K. Ramesha, *ACS Appl. Mater. Interfaces*, 2018, **10**, 19721–19729.
26 S. Zhu, M. Tang, Y. Wu, Y. Chen, C. Jiang, C. Xia, S. Zhuo, B. Wang and C. Wang, *Sustainable Energy Fuels*, 2019, **3**, 142–147.